

The Dual Role of Cerebral Autoregulation and Collateral Flow in the Circle of Willis after Major Vessel Occlusion

Flora Kennedy McConnell and Stephen Payne

Abstract—Objective: Ischaemic stroke is a leading cause of death and disability. Autoregulation and collateral blood flow through the circle of Willis both play a role in preventing tissue infarction. To investigate the interaction of these mechanisms a one-dimensional steady state model of the cerebral arterial network was created. **Methods:** Structural variants of the circle of Willis that present particular risk of stroke were recreated using a network model coupled with: (1) a steady state physiological model of cerebral autoregulation; (2) one wherein the cerebral vascular bed was modelled as a passive resistance. Simulations were performed in various conditions of internal carotid and vertebral artery occlusion. **Results:** Collateral flow alone is unable to ensure adequate blood flow ($> 90\%$ normal flow) to the cerebral arteries in several common variants during internal carotid artery occlusion. However, compared to a passive model, cerebral autoregulation is better able to exploit available collateral flow and to maintain flows within 10% of baseline. This is true for nearly all configurations. **Conclusion:** Hence, autoregulation is a crucial facilitator of collateral flow through the circle of Willis. **Significance:** Impairment of this response during ischemia will severely impact cerebral blood flows, and tissue survival, and hence autoregulation should be monitored in this situation.

I. INTRODUCTION

DURING stenosis or occlusion of an artery supplying the brain, the health of cerebral tissue is primarily dependent on the severity and duration of ischemia. This is because brain tissue has only very small stores of glucose [1], so reductions in cerebral blood flow rapidly lead to a depletion of energy stores, resulting in tissue damage. The head receives around 15% of the total cardiac output [2]; blood is supplied to the brain via the circle of Willis (Figure 1a), an arterial ring at the base of the cranium. Oxygenated blood arrives in the circle of Willis through the four inflow (afferent) arteries. Anteriorly, these are the left and right internal carotid arteries (ICAs) and posteriorly, the left and right vertebral arteries (VAs), which anastomose to form the basilar artery (BA). From the circle of Willis, blood is distributed to the brain tissue via the outflow (efferent) arteries: the left and right anterior, middle and posterior cerebral arteries (ACAs, MCAs and PCAs respectively). The anterior and posterior parts of the circle of Willis are connected by the posterior communicating arteries

(PCoAs), and the ring structure is completed by the anterior communicating artery (ACoA) which connects the left and right sides [3]. Although not shown in the schematic (Figure 1a), most of the arteries of the circle of Willis give rise to further small arteries along their lengths. Along the VAs and BA these small arteries supply blood to structures in the neck and low-lying structures in the head [3].

Figure 1a shows the anatomically ideal structure of the circle of Willis. However, between individuals there is considerable variability in the structure of the circle. A study by Alpers *et al.* [4] examined 350 human brains with no evidence of vascular pathology, other than atherosclerosis, and found that only 52% possessed the complete circle [4]. Another investigation, by Riggs *et al.* [5], examined the brains of 994 patients who had presented with signs of neural dysfunction, and found that only 19% of the group had a complete circle of Willis [5]. Particularly common structural variations include: absence of one, or both, of the PCoAs; absence of the proximal segment of one ACA (the ACAA1); and absence of the proximal segment of one PCA (the PCAP1). Each of these structural variations occurs in around 10% of people [6]. It is through the seemingly redundant communicating arteries that the circle of Willis thus provides the brain with primary collateral (i.e. alternative) flow pathways. These pathways potentially enable blood to bypass a vessel blockage and to continue to supply hypoperfused tissue [7], thereby reducing the severity of ischemia.

As a result of this complex behaviour, there have been many attempts to model the cerebral arterial network. In 1986 Hillen *et al.* [8] used a non-linear 1D model of a well-balanced circle of Willis to show that flows into and around the circle are dominated by vessel resistances, which increase as vessel cross-section decreases. Flows away from the circle are dominated by peripheral resistances, which represent the resistance of the downstream arterial and capillary networks. In 2007 Alastruey *et al.* [9] included elastically-varying arterial walls in the 1D model used by Hillen *et al.* [8]. They used their model to examine the effects of common anatomical variations of the circle of Willis on cerebral blood flows. Studies by Devault *et al.* [10] and Perdikaris *et al.* [11] have since produced 1D models of the network in which the arterial walls respond viscoelastically.

However, these models have neglected the effects of

F. Kennedy McConnell and S. Payne are with the Department of Engineering Science, University of Oxford, Parks Road, Oxford, UK, OX1 3PJ e-mail:flora.kennedy-mcconnell@eng.ox.ac.uk. Manuscript received April 22nd 2016. Copyright (c) 2016 IEEE. Personal use of this material is permitted. However, permission to use this material for any other purposes must be obtained from the IEEE by sending an email to pubs-permissions@ieee.org.

taken here to be 4.5 *mPas* [9].

Using Poiseuille's equation, the arterial network shown in Figure 1 of [9] becomes analogous to a series of interconnected resistances, the circle of Willis portion of which is shown in Figure 1b. In this structure, each of the terminal arteries (the brachials, the thoracic aorta, the external carotids, and the cerebral arteries) is coupled to a peripheral resistance which accounts for the total resistance of the arterial network between the terminal vessel and the venous system. The peripheral resistances were used to calculate the pressures and flow rates at the distal ends of the terminal arteries:

$$p = p_v + R_p Q \quad (2)$$

where p_v is the pressure of the venous system, which, as in Alastruey *et al.* [9], was taken to be 5 *mmHg* (666.7 *Pa*).

The network model was then adapted to take account of CBF autoregulation by the brain's arteriolar network. This involved adapting the peripheral resistances coupled to the cerebral arteries (the resistances shown in dashed boxes in Figure 1b) using the small artery, capillary, and venous components of the autoregulation equivalent circuit of Payne [24].

At steady state the Payne model (Figure 2a) condenses to two resistances connected in series: a variable resistance, representing the small arteries and arterioles; and a fixed resistance, representing the capillaries, and the small and large veins (Figure 2b). The peripheral resistances from the non-autoregulating model were thus replaced with the resistances in Figure 2b. In order to match the autoregulating and non-autoregulating network models, under baseline conditions it was assumed that $\bar{R}_{sa} + R_v = R_p$, where R_{sa} is the variable resistance of the regulating small arteries and arterioles, and \bar{R}_{sa} represents its baseline value. Also $R_v = R_{sv} + R_{lv}$, where R_{sv} is the resistance of the capillaries and small veins, and R_{lv} is the resistance of the large veins. The partitioning of the peripheral resistances was done by matching the ratios of $\bar{R}_{sa}:R_v$ used by Payne [24].

The resistance of a blood vessel is related to its radius, according to equation 1; in the autoregulation model a vessel's resistance is thus assumed to be related to its volume by:

$$\frac{V_{sa}}{\bar{V}_{sa}} = \sqrt{\frac{R_{sa}}{\bar{R}_{sa}}} \quad (3)$$

where V_{sa} is the volume of the arteriolar compartment and \bar{V}_{sa} denotes its value under baseline conditions.

Arterial compliance, C_a relates the rates of change of arterial volume and pressure:

$$\frac{dV_{sa}}{dt} = \frac{d[C_a \cdot (P_1 - P_{ic})]}{dt} \quad (4)$$

which, at steady-state, reduces to:

$$V_{sa} - \bar{V}_{sa} = C_a \cdot [(P_1 - P_{ic}) - (\bar{P}_1 - P_{ic})] \quad (5)$$

where P_{ic} is the intracranial pressure and P_1 is the pressure of the arteriolar compartment.

Cerebral blood flow is regulated by adjusting the compliance

of the arteriolar compartment based on a negative feedback parameter proportional to the deviation in flow from baseline. Payne [24] modelled this change in arteriolar compliance using an asymmetrical sigmoidal curve:

$$C_a = \bar{C}_a + \frac{1}{2} \begin{cases} \Delta C_a^+ \tanh\left[-\frac{2G_q}{\Delta C_a^+} \left(\frac{q-\bar{q}}{\bar{q}}\right)\right], & \text{if } q < \bar{q} \\ \Delta C_a^- \tanh\left[-\frac{2G_q}{\Delta C_a^-} \left(\frac{q-\bar{q}}{\bar{q}}\right)\right], & \text{if } q > \bar{q} \end{cases} \quad (6)$$

where \bar{C}_a is the baseline arterial compliance. ΔC_a^+ and ΔC_a^- define the upper and lower limits on the value of compliance respectively, \bar{q} is the baseline healthy flow through the afferent artery, and G_q is the gain of the flow feedback mechanism. Thus, an equation relating P_{in} , pressure at the distal end of a cerebral artery, to q , flow through that artery can be found:

$$\left[\frac{P_{in} - P_v - qR_v}{q} \right] \cdot [C_a(P_{in} - 2P_{ic} + P_v + qR_v) - \bar{C}_a(2\bar{P}_{in} - 2P_{ic} - \bar{q}\bar{R}_{sa}) + 2\bar{V}_{sa}]^2 - 4\bar{R}_{sa}\bar{V}_{sa}^2 = 0 \quad (7)$$

Equation 7 can be solved numerically to calculate q for any value of the arterial input pressure P_{in} .

Numerical solution: At arterial bifurcations and junctions the pressure was set to be equal in all vessels at each node. The pressure at all but the first and last nodes in the network is thus given by a linear equation of the form:

$$\sum_{i=2}^{n-1} (P_i - P_j) G_{ij} = S_i \quad (8)$$

where G_{ij} is the flow conductance of a vessel connecting node i to every other node j . If i is not connected to a node j then $G_{ij} = 0$. S_i is a source term equal to the net blood flow at node i . Due to conservation of mass this term should be zero for all nodes other than those at the input (the start of the aorta), and the output to the venous system. However, rather than fixing these flows as boundary conditions, modified nodal analysis was used to impose pressure boundary conditions at the input and outputs of the network. This system of linear equations was put into the following matrix form:

$$\mathbf{BP} = \mathbf{S} \quad (9)$$

where \mathbf{B} is a matrix of vessel conductance terms, vector \mathbf{P} contains the pressure at each node, and \mathbf{S} is the vector of source terms. In matrix form:

$$\begin{bmatrix} \sum_n G_{11} & -G_{12} & \cdots & -G_{1n} & 1 & 0 \\ -G_{21} & \sum_n G_{22} & \cdots & -G_{2n} & 0 & 0 \\ \vdots & \vdots & \ddots & \vdots & \vdots & \vdots \\ -G_{(n-1)1} & \cdots & \cdots & -G_{(n-1)n} & 0 & 0 \\ -G_{n1} & \cdots & \cdots & \sum_n G_{nn} & 0 & 1 \\ \hline 1 & 0 & \cdots & 0 & 0 & 0 \\ 0 & 0 & \cdots & 1 & 0 & 0 \end{bmatrix} \begin{bmatrix} P_h \\ P_2 \\ \vdots \\ P_{n-1} \\ P_n \\ \hline S_1 \\ S_n \end{bmatrix} = \begin{bmatrix} S_1 \\ S_2 \\ \vdots \\ S_{n-1} \\ S_n \\ \hline P_h \\ P_n \end{bmatrix} \quad (10)$$

The rows of matrix \mathbf{B} below the horizontal dashed line allow the inclusion of pressure boundary conditions at the input and outputs of the network. The columns to the right of the vertical dashed line allow the inflow S_1 and outflow S_n to

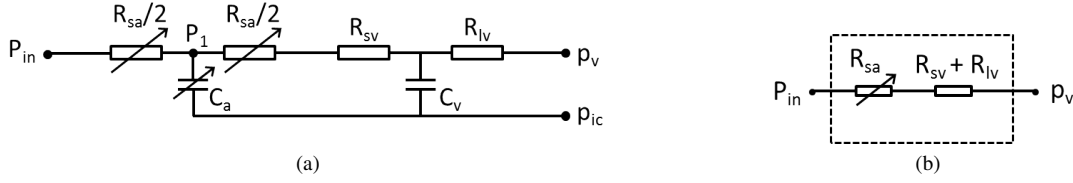


Fig. 2. Electrical equivalent circuit representations of the autoregulation model of Payne [24]: a) the full dynamic model; and b) its steady state equivalent.

be included as parameters to be found, rather than boundary conditions. Finding vector \mathbf{P} involves inversion of this matrix equation by Gaussian elimination. The resulting node pressure values are then used to find the flow rates of blood in every artery in the network.

The autoregulation model was expressed in matrix form, in the same way as in equation 10. The pressure at the start of the aorta, P_h , and the venous pressure remained as boundary conditions. However, the pressure at the distal end of each of the cerebral arteries was calculated using equation 7 and imposed in the matrix system in the same way as the boundary conditions, i.e. in equation 10 the flow rates were included as additional rows below the dashed line in the \mathbf{P} vector, with the calculated corresponding pressures imposed below the dashed line in the \mathbf{S} vector. The autoregulation matrix equation, and equation 7, were then solved iteratively, according to the scheme given in the supplementary material.

Parameter values: The parameters used to create the network model: vessel lengths and radii and peripheral resistances, were taken from Alastruey *et al.* [9]. For arteries below the circle of Willis, vessel length and radius data were taken from the work of Stergiopoulos *et al.* [25]; for the arteries of the circle of Willis the data were taken from Fahrig *et al.* [26]. The peripheral resistance values were calculated by Alastruey *et al.* [9] assuming that the distal end of each cerebral artery is coupled to a three-element model consisting of a resistance, R_1 , in series with a parallel combination of a second resistance, R_2 and a capacitor. The values of R_1 were fixed to the characteristic impedances of the associated terminal arteries. To determine the values of R_2 the total resistance of the arterial network was taken to be $R_T = 1.34 \times 10^8 \text{ Pa s m}^{-3}$ [25] and the peripheral resistances $R_p = R_1 + R_2$ apportioned, such that 15% of the cardiac output goes to the head, 5% goes to each arm, and 75% goes to the rest of the body [9]. The blood flow to the head was split between the six cerebral arteries and the two external carotid arteries in proportion to the initial cross-sectional area of the associated terminal artery. In this work the inlet pressure at the aorta (P_h) was determined as the pressure that provided cardiac output, through the healthy ‘full circle’ network, equal to the time average of the cardiac output flow function used by Alastruey *et al.* [9].

The parameters used to define the autoregulatory model: $\overline{C_a}$, ΔC_a^+ , ΔC_a^- , $\overline{V_{sa}}$, and G_q , were taken from Payne [24]. However, the parameter values Payne used represent the arterioles supplying the whole brain. In this work a scaled down version of this model was connected to each of the cerebral arteries;

representing the vascular networks beyond the circle of Willis. Hence, each of the model parameters was scaled down. For $\overline{V_{sa}}$ this was done using equation 3 and the values of $\overline{R_{sa}}$, which were calculated from the peripheral resistances of the non-autoregulating model. Then, the remaining autoregulation model parameters were scaled down by the same proportion as $\overline{V_{sa}}$. The resulting parameter values used to define the autoregulating part of the model are given in Table I.

Simulations: As already discussed, the structure of the circle of Willis is widely variable. One key aim of this work was to investigate the effect of variations in the structure of the circle of Willis on its capacity for collateral flow. The circle configurations considered were those identified by Papantchev *et al.* [19]. Two additional, commonly occurring networks were included [6]: both PCoAs absent; and one PCoA absent with the contralateral PCA P1 segment also absent. All of the variants considered are listed in Table II. For every one of the circle variants the arterial network model was used to:

- 1) Examine the flows through the cerebral and communicating arteries under baseline conditions, i.e. when none of the afferent arteries was occluded.
- 2) For both the non-autoregulating and the autoregulating versions of the model: to examine the effect of the following occlusion conditions:
 - a) Partial occlusion of the LICA
 - b) Total occlusion of the LICA
 - c) Total occlusion of the LVA
 - d) Partial occlusion of the LICA and total occlusion of the RICA
 - e) Total occlusion of the LICA and partial occlusion of the RICA

on the outflows through the cerebral arteries, for the reasons described below.

Partial occlusion was defined by a reduction in ICA radius to 50% of its healthy value. This definition was chosen as it is the lower bound on the degree of stenosis for which carotid endarterectomy has been found to be beneficial [27]. Total occlusion of the LICA and the LVA were both considered individually because the circle of Willis geometries under investigation are those that were identified by Papantchev *et al.* [19] as being at high risk of cerebral ischemia during disruption of the supply to the left side of the circle. Combinations of stenosis and occlusions of both internal carotid arteries were also considered, because atherosclerosis of the carotid arteries is generally bilaterally symmetrical [28]. Moreover, a carotid endarterectomy procedure to reduce stenosis in one ICA would involve occlusion of that ICA and,

TABLE I
AUTOREGULATION MODEL PARAMETER VALUES

Parameter	$\overline{V_{sa}}$	G_q	$\overline{C_a}$	ΔC_a^+	ΔC_a^-	$\overline{R_{sa}}$	R_v	P_h	P_v	P_{ic}
Units	ml	ml/mmHg	ml/mmHg	ml/mmHg	ml/mmHg	mmHg s/ml	mmHg s/ml	mmHg	mmHg	mmHg
MCAs	4.71	1.18	0.08	1.13	0.06	32.60	12.18	—	—	—
PCAs	3.46	0.87	0.06	0.83	0.05	60.50	22.61	—	—	—
ACAs	3.96	0.99	0.07	0.95	0.05	46.31	17.30	—	—	—
Whole network	—	—	—	—	—	—	—	108	5	10
Payne [24]	12	3.0	0.21	2.87	0.16	5.03	1.88	—	6	10

therefore, reliance on collateral flow through the circle of Willis from the contralateral ICA, which may also be stenosed.

The model was also used to replicate the carotid endarterectomy simulations carried out by Liang *et al.* [18]. In the 2011 study stenotic conditions were simulated, then once the network had reached steady state the autoregulating cerebral resistances were fixed, and one of the ICAs was widened. In the current work Liang's five stenotic conditions: LICA, RICA, bilateral ICA, concurrent BA and LICA, and concurrent BA and RICA stenoses, were simulated in the nine circle of Willis geometries considered in [18]. Stenosis was modelled as a 60% reduction in vessel radius. Any circle in which a cerebral territory saw a flow increase of $> 100\%$ after ICA widening was considered to be at risk of cerebral hyperperfusion.

III. RESULTS

Table II lists the 'healthy' flow rates of blood through the efferent and communicating arteries in various configurations of the circle of Willis. The values given are those calculated using the non-autoregulating version of the cerebrovascular network. These flows were then taken to be the baseline condition for the autoregulating version of the model. The 'no collateral flow' (variant 13) network refers to a circle of Willis configuration that lacks the posterior and anterior communicating arteries; thereby completely lacking capacity for collateral flow.

In Table II the circle that produced the greatest deviations from the 'full circle' flows was found to be variant 10: a circle missing the A1 segment of the RACA and the P1 segment of the LPCA. The vessel in variant 10 with the lowest flow relative to its value for variant 1 is the LPCA, which rather than being fed by the vertebrals, is fed by the LICA, via the LPCoA. However, it received 1.00 ml s^{-1} of blood, a reduction of only 8.3% from the 1.09 ml s^{-1} received by the LPCA in variant 1, illustrating the robustness of the collateral network.

Figure 3 shows the effect of occlusion of the LICA on flows through the efferent arteries of the complete, well balanced circle of Willis (variant 1). Total occlusion is indicated by the solid black cross. The grey numbers next to each artery give the percentage **reductions** in flow through that artery, found using the autoregulation model, relative to the no-occlusion 'healthy' flows given for variant 1 in Table II. The black numbers give the corresponding percentage reductions in

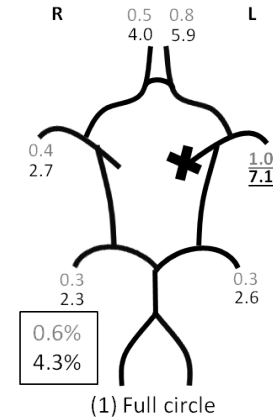


Fig. 3. Percentage reductions in the flow rates through the cerebral arteries of the full circle of Willis (variant 1 in Table II) during total LICA occlusion (denoted by a solid black cross). The maximum reduction in each case is underlined. The boxed numbers give the total percentage reduction in flow to the brain. Grey numbers denote an autoregulating vascular bed, and black numbers denote a passive vascular bed.

flow from simulation using the non-autoregulating model. For example, Figure 3 shows that, when the LICA of variant 1 is occluded, the largest drop in flow rate is found in the LMCA, where it **falls** by 7.1% without the effect of autoregulation, but by only 1.0% when autoregulation is included.

Figure 4 shows the effects of LICA occlusion on the flows in the efferent arteries of the remaining circle of Willis geometries under consideration (note that for variant 13, 75% area reduction was applied, rather than total occlusion). From Figure 4 it is evident that autoregulation enables improved maintenance of blood flow to the cerebral tissue. This is true for all networks where there is some capacity for collateral flow (see supplementary material for the remaining occlusion conditions), i.e. excluding the networks in Figures 4g and 4i, in which the blood supply to the brain was reduced by 38.0% and 63.8% respectively. These are the two most vulnerable networks: in variant 8 (Figure 4g) both the left middle and anterior cerebral territories, and in variant 10 (Figure 4i) the entire left hemisphere and the right anterior cerebral territory are at very high risk of ischemia.

Figure 5 shows several simulations of network 10. 'Partial occlusion' refers to a reduction of vessel radius to 50% of

TABLE II

FLOW IN THE EFFERENT AND COMMUNICATING ARTERIES OF THIRTEEN CIRCLE OF WILLIS GEOMETRIES. THE NUMBERS IN THE LEFT-MOST COLUMN ARE USED TO REFER TO DIFFERENT NETWORK VARIANTS LATER IN THE TEXT AND FIGURES. FLOW VALUES ARE GIVEN IN mls^{-1} . NEGATIVE VALUES OF FLOW INDICATE THAT THE DIRECTION OF FLOW IS REVERSED RELATIVE TO THE POSITIVE DIRECTION INDICATED IN FIGURE 1B.

Variant	Description	Cerebral arteries						Communicating arteries		
		LMCA	RMCA	LACA	RACA	LPCA	RPCA	LPCoA	RPCoA	ACoA
1	Full circle	2.06	2.06	1.42	1.42	1.09	1.09	0.06	0.03	-0.07
2	No LPCoA	2.06	2.06	1.42	1.42	1.10	1.10	—	0.05	-0.09
3	No ACoA	2.06	2.06	1.42	1.42	1.09	1.09	0.07	0.02	—
4	No RVA	2.05	2.05	1.42	1.42	1.08	1.08	-0.23	-0.26	-0.07
5	No LPCAP1	2.04	2.06	1.41	1.42	1.03	1.10	-1.03	0.39	-0.49
6	No RACAA1	2.03	2.10	1.39	1.37	1.09	1.10	0.37	-0.28	1.37
7	No PCoAs	2.06	2.06	1.42	1.42	1.10	1.10	—	—	-0.08
8	No ACoA or LPCoA	2.06	2.06	1.42	1.42	1.10	1.10	—	0.03	—
9	No ACoA or RVA	2.05	2.06	1.41	1.42	1.08	1.08	-0.21	-0.27	—
10	No RACAA1 or LPCAP1	1.99	2.11	1.36	1.34	1.00	1.12	-1.00	0.10	1.34
11	No RACAA1 or RVA	2.02	2.09	1.38	1.37	1.07	1.08	0.08	-0.57	1.37
12	No LPCoA or RPCAP1	2.05	2.04	1.41	1.41	1.12	1.03	—	-1.03	0.21
13	No communicating arteries	2.06	2.06	1.42	1.42	1.10	1.10	—	—	—
Fahrig <i>et al.</i> (range)		2.0 (1.8 – 2.7)		1.1 (1.0 – 1.4)		0.8 (0.7 – 0.9)		—	—	—

the ‘healthy’ value, i.e. a 75% reduction in the vessel area. A dashed line in the circle of Willis drawing is used to denote a circulus vessel whose radius is 50% of the value used when modelling the ‘complete’ circle of Willis (network 1). Figure 5 demonstrates that autoregulation ameliorates the reduction in efferent flows; this is seen in all but the most severe combination of total LICA occlusion, with no capacity for right-side to left-side collateral flow (Figure 5a).

The effect of anterior communicating (Figure 6a), and left posterior communicating (Figure 6b) artery areas on flows through the LACA, LMCA, ACoA and LPCoA, when the LICA is occluded, was examined. The results are shown for both the non-autoregulating model (solid lines) and the autoregulating model (dashed lines). Figure 6a shows that the autoregulating components of the model allow the network to compensate for absence of the ACoA. Flow through the LPCoA is raised to more than 3 times its value when the ACoA is present, meaning that flows through the cerebral arteries are maintained within 3% of their values when variant 1 is subjected to LICA occlusion. Hence, the autoregulating version of the network model is better able to make use of the collateral flow route through the LPCoA in order to maintain flows to the cerebral arteries at near their healthy levels.

As the area of the ACoA increases from 10 – 90%, of its ‘healthy’ state, its flow capacity increases sharply, levelling off thereafter. At an area of 45%, the ACoA becomes the dominant collateral flow route to the LACA and LMCA. The same effect is evident in the LPCoA (Figure 6b), however, absence of the LPCoA is less detrimental to flows through the LACA and LMCA during LICA occlusion, than absence of the ACoA. Additionally, the LPCoA does not become the dominant collateral flow route until its area is increased to approximately 180% of its ‘healthy’ value.

The results of simulations replicating those of Liang *et al.* [18] are given in the supplementary materials (Tables 2-7). The circle variants that saw large efferent flow increases after carotid endarterectomy are circles 7, 8 and 12, and an additional circle missing the RACAA1 and RPCAP1 segments.

IV. DISCUSSION

The results of simulations of ‘healthy’ networks, i.e. those in which the radii of the four afferent arteries of the circle of Willis were unchanged (Table II), showed that absence of one, or even two, of the circulus arteries did not reduce the efferent flows through the cerebral arteries by more than 10%. The efferent flow rates themselves bear reasonable similarity to the values presented in Fahrig *et al.* [26], which are weighted averages of values obtained from a literature review of measurement studies estimating flow rates of blood entering and exiting the circle of Willis. Some differences between measured estimates of flow rates, and those from the simulations carried out in this work, were expected. This is because the simplified structure of the circle of Willis modelled here does not take account of the small perforating arteries that arise from its segments. These vessels include, for example, the spinal artery, which arises from the vertebral arteries, and the cerebellar and pontine arteries, all of which arise from the basilar artery. Hence, the measurements averaged by Fahrig *et al.* [26] estimate that 11.8 mls^{-1} enter the circle of Willis and 7.8 mls^{-1} leave via the cerebral arteries, whereas, the model presented here sees 9.1 mls^{-1} passing into and out from the full circle under healthy conditions. While the perforating arteries were omitted for simplicity in this study, it would be possible to include them in the network model; furthermore, doing so may bring the posterior cerebral artery flow rates down into the range of measured values presented in Fahrig *et al.* [26].

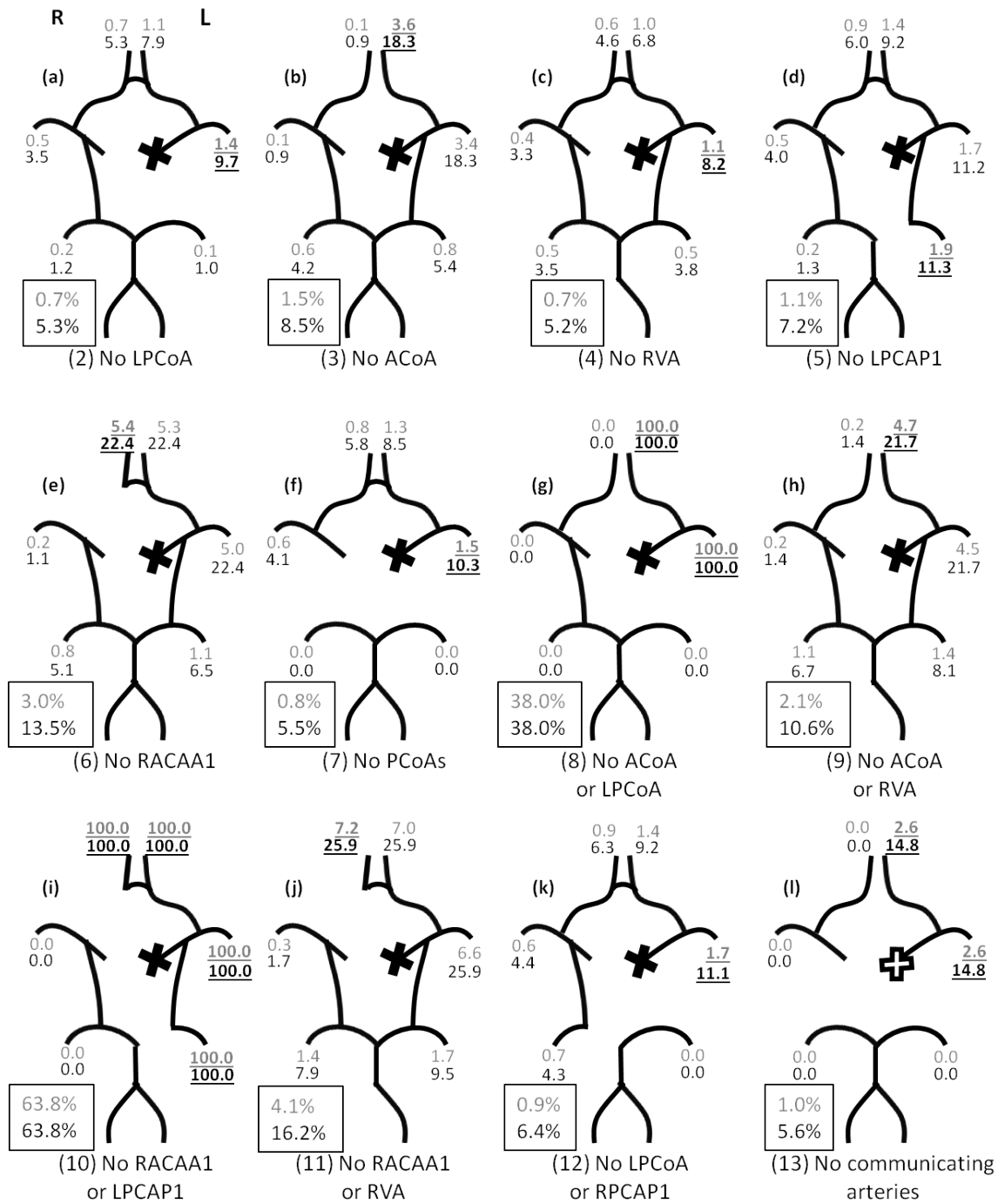


Fig. 4. Percentage reductions in flow rates through the cerebral arteries of various circle of Willis configurations. A solid black cross denotes total occlusion of an artery, whereas a hollow cross indicates 75% area reduction. Grey numbers give the percentage flow reductions found from simulations using the autoregulation model. Black numbers are the percentage flow reductions that result when autoregulation is not taken into account. The maximum reduction in each case is underlined. The boxed numbers give the total percentage reduction in flow to the brain. Full data and network risk classifications are provided in the supplementary materials.

Between modelling studies there are differences in the total blood flow through the circle of Willis, which makes direct comparison of efferent flow rates difficult. In most cases the difference in total flux is due to differences in arterial geometries, boundary conditions, and peripheral resistances. Several models [14], [15], [29], [30] have assigned the peripheral resistances of the cerebral territories based on their

relative masses, such that the $R_{ACA} : R_{MCA} : R_{PCA}$ ratio is 6 : 3 : 4. This results in greater flow through the PCAs than the ACAs, an assumption that is not supported by the data of Fahrig *et al.* [26]. Alastruey *et al.* [9] report lower flow through the circle of Willis which is likely due to the fact that the arteries below the neck were modelled as more compliant than those in the neck and the circle of Willis. As a vessel's

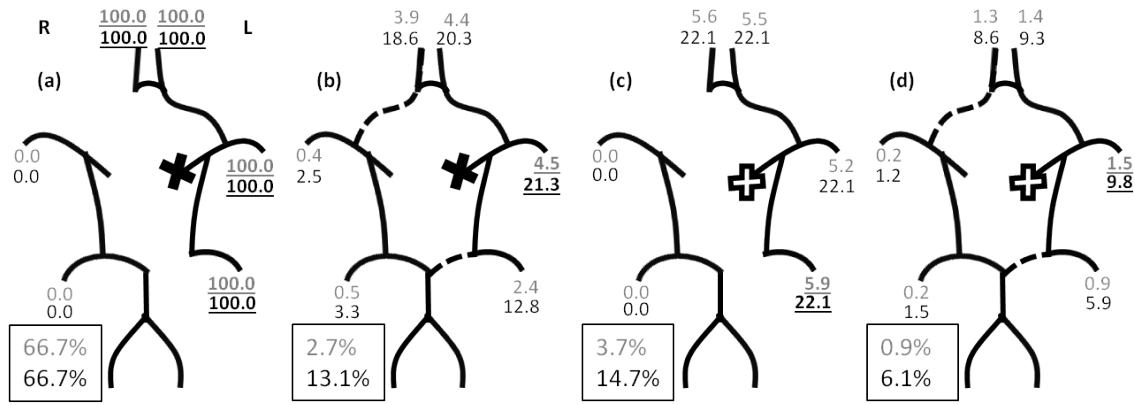


Fig. 5. Percentage reductions in flow rates through the cerebral arteries of the circle of Willis in which the proximal segments of the RACA and the LPCA are absent or hypoplastic (variant 10). A solid black cross denotes total occlusion, whereas a hollow cross indicates a 75% reduction in area. A dashed vessel line indicates that an arterial segment is hypoplastic (75% area reduction). a) Total LICA occlusion in circle with absent RACAA1 and LPCAP1. b) Total LICA occlusion in circle with hypoplastic RACAA1 and LPCAP1. c) Partial LICA occlusion in circle with absent RACAA1 and LPCAP1. d) Partial LICA occlusion in circle with hypoplastic RACAA1 and LPCAP1. The maximum reduction in each case is underlined. Boxed numbers give the total percentage reduction in blood supplied to the brain. Flow reductions: grey numbers = autoregulating model, black numbers = non-autoregulating model.

steady-state resistance (equation 1) varies non-linearly with radius this leads to a greater reduction of the time-averaged resistance relative to the steady-state resistance in these vessels, than occurs in the cerebral vessels, an effect which thereby draws blood away from the head.

There are large variations in the flows through the communicating arteries. In the ‘full circle’ geometry the flows in these vessels are two orders of magnitude lower than the flows through the efferent vessels. This fact, along with the normal cerebral flows in variant 13, indicates that in the absence of afferent vessel occlusion the complete circle of Willis does not require the communicating arteries in order to adequately supply all six cerebral arteries. However, in certain circle variants, under normal afferent vessel conditions, the flows through the communicating arteries can be 30 – 40 times their values in variant 1; indicating substantial redundant flow capacity. Hence, some of the circle variants rely on collateral flow through the communicating arteries. The circle of Willis configuration in which the efferent flows are most affected under healthy conditions is the one missing the proximal segments of both the RACA and the LPCA (variant 10), which was detected in < 1% of the circles examined by Papantchev *et al.* [19]. In this variant of the circle, the distal RACA and LPCA are both supplied by collateral flow from the LICA, via the ACoA and the LPCoA, respectively. Hence, the LICA carries the blood supply to all three left-sided cerebral territories, as well as the RACA territory. This cerebral tissue is, therefore, at very high risk of ischemia in the event of LICA stenosis or occlusion, as the blood flow to the brain is reduced by 63.8%. This circle configuration was identified by Papantchev *et al.* [19] as one of the most high risk variations of the circle of Willis structure.

Figure 4 shows that blood flow rates through the cerebral arteries fall under conditions of ICA occlusion. Without the effect of autoregulation, most of the circle of Willis configurations considered see a flow reduction of > 10%

in at least one of the efferent arteries. The circle variants that were less severely affected were 1, 2, and 4, which therefore present a low risk of ischemia when subjected to LICA occlusion. However, cerebral autoregulation is able to substantially mitigate flow deficits, i.e. limit them to flow reductions of < 10%, in circle variants 3, 5, 6, 7, 9, 11, and 12. This is because cerebral flow deficits trigger reductions in the R_{sa} values of the autoregulation models coupled to the cerebral arteries, thereby drawing blood through the circle of Willis to these arteries. Hence, these circle variants present a moderate risk of ischemia under LICA occlusion. The only circle of Willis geometries whose flow reductions were not ameliorated by autoregulation were variants 8, 10 and 13. These are networks which lack an exploitable collateral flow route to the LMCA and LACA and, therefore, present a high risk of tissue ischemia when the LICA is occluded. In these cases the blood supply to the brain is reduced by 38.0%, 63.8%, and 38.0% respectively. It should be noted that autoregulation has been assumed to be spatially uniform, meaning that the vascular beds downstream of the cerebral arteries have been modelled as either all autoregulating or all passive, which may not be the case *in vivo*.

Results of modelling the complete circle of Willis show good agreement with previous studies that have included a model of cerebral autoregulation. For example, the model very closely replicates the results shown in Fig. 4 of Moorhead *et al.* [15]. The main difference is a lower supply of blood to the posterior circulation in the current work due to higher peripheral resistances distal to the posterior cerebral arteries, and lower blood pressures at the proximal ends of the VAs relative to the ICAs. However, the works of [14], [15], [29], and [30] demonstrate autoregulatory control returning efferent flow rates to their reference values in most studied anatomical variants, after a pressure drop in an ICA, results which the modelling work presented here does not reproduce (Figure 4). This is due to two differences between the models: firstly, the current work

simulates ICA occlusion by setting $r = 0$ when calculating the vessel's resistance rather than reducing a pressure boundary condition proximal to the ICA. Secondly, the values of the autoregulating peripheral resistances are constrained within this physiological model by the limits of the function for arteriolar compliance (equation 6). In the case of LICA occlusion the greatest changes in the peripheral resistances are seen in the ACA territories of circle of Willis variant 11, which reduce to $R_{sa} + R_v = 0.69R_p$. This explains the good agreement with the results of [17], in which the peripheral resistances were constrained to: $0.74R_p < R < 1.30R_p$. In contrast, the models of [14], [15], [29], and [30] constrain the peripheral resistances to $0.05R_p < R < 1.95R_p$, providing the cerebral territories with a greater ability to draw blood through the low pressure ICA and the communicating arteries.

The results of carotid endarterectomy simulations are in agreement with the results of Liang *et al.* [18] as the current model identifies the same circle of Willis structures as high risk. The results differ slightly in the case of concurrent BA and ICA stenosis, possibly due to differences in the physiological data used to create the two models. The current model identifies only circle 8 as high risk when the BA and LICA are stenosed, and only the additional circle in which the RACAA1 and RPCAP1 are absent as high risk when the BA and RICA are stenosed. The flow rates in the two circle structures each only reach the 'high risk' threshold in one case of concurrent BA and ICA stenosis. However, both circles cause substantial increases in flow irrespective of which ICA is occluded. The general agreement between the two models supports the use of the Poiseuille equation as an approximation to the steady state 1D flow equation.

Figure 5 demonstrates that the presence of an available blood flow route, be it through a stenosed LICA, or through narrow proximal ACA and PCA segments, permits autoregulation to return efferent flows to within 6% of their baseline rates. Additionally Figure 6 shows that if a vessel's area is greater than around 25% of its healthy value it can permit blood flow at a high enough rate to affect flows through the downstream cerebral arteries. The figure indicates that in the event of LICA occlusion, the ACoA is the more valuable collateral route, which is in agreement with previous modelling studies [9], [29]. Figures 6a and 6b also show that the potential flow capacities of the ACoA and the PCoAs are greater than 3 ml s^{-1} , which is up to 100 times the flow rates in these vessels in variant 1, under healthy conditions. This is in agreement with the notion that the communicating arteries are redundant collateral vessels, which are 'recruited' when required. It has been shown using transcranial Doppler measurements during carotid endarterectomy, that this 'switching-on' of collateral vessels can occur within two or three heartbeats [20]. It may be that fortification of these newly recruited collateral routes then occurs, through vessel remodelling, over a period of weeks [20], although this remains very poorly understood.

The model presented here has provided insight into the

importance of collateral flow pathways and autoregulation in the maintenance of cerebral blood flows during afferent vessel occlusion. It is novel in that it incorporates a model of cerebral autoregulation, enacted through peripheral resistance variations, which are brought about by pressure induced changes in arteriolar compliance. Most prior attempts to model autoregulation in the peripheral resistances of the cerebral arterial network have used PID control techniques without modelling the physiological mechanism that causes vasodilation and vasoconstriction of the cerebral arterioles, whereas the network model in this study is based on physiological data measured in healthy young adults [9]. The main limitations of this study lie in its lack of specificity to individual subjects and the lack of experimental validation. Detailed, patient-specific information on arterial geometry, arteriolar resistance, and network boundary conditions is lacking. Hence, in order to provide information about individual patients, personalisation with subject specific measurements will be required.

V. CONCLUSION

There is evidence to support the hypothesis that the presence of good collateral flow routes on angiography can indicate: a lower risk of stroke [31]; a greater chance of successful recanalisation therapy [22]; a lower risk of haemorrhagic transformation after recanalisation therapy [23]; and a smaller infarct volume [21]. However, this work shows that the status of the arteriolar network's autoregulatory ability is also vitally important when assessing collateral flow, and may be just as good a predictor of ischemic disease risk and cerebrovascular intervention outcomes. Autoregulation should, therefore, be quantified alongside collateral status in a clinical context. This is particularly true in certain circle variants, which have been shown to be strongly affected by autoregulation. Finally, the cerebrovascular network model developed here could prove a useful tool for patient assessment and treatment planning, through identification of good candidates for interventions such as carotid endarterectomy, and recanalisation therapies.

ACKNOWLEDGEMENT

FKM gratefully acknowledges support from RCUK Digital Economy Programme grant number EP/G036861/1 (Oxford Centre for Doctoral Training in Healthcare Innovation).

REFERENCES

- [1] H. Markus, "Cerebral perfusion and stroke," *Journal of Neurology, Neurosurgery & Psychiatry*, vol. 75, no. 3, pp. 353–361, 2004.
- [2] L. R. Williams and R. W. Leggett, "Reference values for resting blood flow to organs of man," *Clinical Physics and Physiological Measurement*, vol. 10, no. 3, p. 187, 1989.
- [3] A. Crossman and D. Neary, *Neuroanatomy: An Illustrated Colour Text*. Edinburgh: Elsevier Churchill Livingstone, 2014, pp. 62.
- [4] B. J. Alpers, R. G. Berry, and R. M. Paddison, "Anatomical studies of the circle of Willis in normal brain," *Archives of Neurology and Psychiatry*, vol. 81, no. 4, p. 409, 1959.
- [5] H. E. Riggs and C. Rupp, "Variation in form of circle of Willis: the relation of the variations to collateral circulation: anatomic analysis," *Archives of Neurology*, vol. 8, no. 1, p. 8, 1963.
- [6] H. Lippert and R. Pabst, *Arterial variations in man: classification and frequency*. Munich: J. F. Bergmann-Verlag, 1985, pp. 92–93.
- [7] D. S. Liebeskind, "Collateral circulation," *Stroke*, vol. 34, no. 9, pp. 2279–2284, 2003.

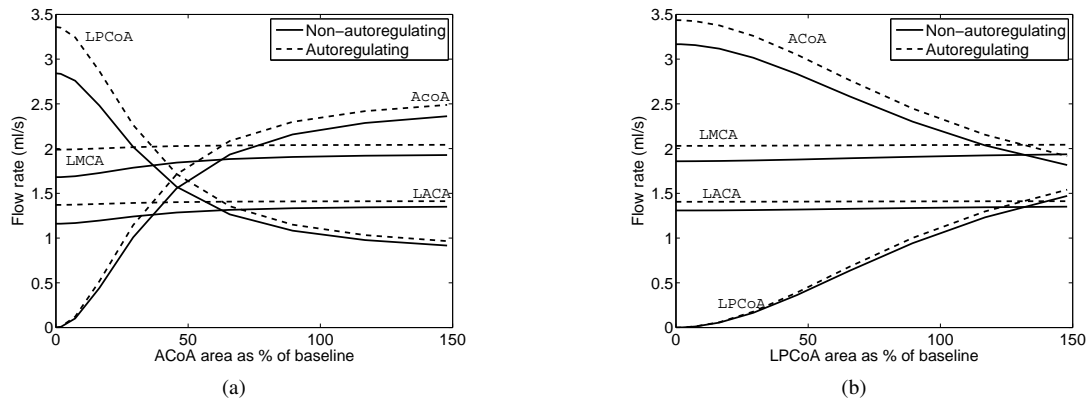


Fig. 6. Flows through the LMCA, LACA, LPCoA and ACoA, in variant 1, during LICA occlusion, shown as a function of: a) ACoA area; b) LPCoA area

- [8] B. Hillen, H. W. Hoogstraten, and L. Post, "A mathematical model of the flow in the circle of Willis," *Journal of biomechanics*, vol. 19, no. 3, pp. 187–194, 1986.
- [9] J. Alastruey, K. H. Parker, J. Peiró, S. M. Byrd, and S. J. Sherwin, "Modelling the circle of Willis to assess the effects of anatomical variations and occlusions on cerebral flows," *Journal of biomechanics*, vol. 40, no. 8, pp. 1794–1805, 2007.
- [10] K. DeVault, P. A. Gremaud, V. Novak, M. S. Olufsen, G. Vernieres, and P. Zhao, "Blood flow in the circle of willis: modeling and calibration," *Multiscale Modeling & Simulation*, vol. 7, no. 2, pp. 888–909, 2008.
- [11] P. Perdikaris, L. Grinberg, and G. E. Karniadakis, "An effective fractal-tree closure model for simulating blood flow in large arterial networks," *Annals of biomedical engineering*, vol. 43, no. 6, pp. 1432–1442, 2015.
- [12] S. K. Piechnik, M. Czosnyka, K. Cieřlicki, and D. Cieřla, "Problems in application of purely linear models in cerebral circulation," *Journal of biomechanics*, vol. 35, no. 4, pp. 553–554, 2002.
- [13] O. Paulson, S. Strandgaard, and L. Edvinsson, "Cerebral autoregulation," *Cerebrovascular and brain metabolism reviews*, vol. 2, no. 2, pp. 161–192, 1989.
- [14] A. Ferrandez, T. David, and M. Brown, "Numerical models of autoregulation and blood flow in the cerebral circulation," *Computer Methods in Biomechanics & Biomedical Engineering*, vol. 5, no. 1, pp. 7–19, 2002.
- [15] K. T. Moorhead, C. V. Doran, J. G. Chase, and T. David, "Lumped parameter and feedback control models of the auto-regulatory response in the circle of Willis," *Computer Methods in Biomechanics and Biomedical Engineering*, vol. 7, no. 3, pp. 121–130, 2004.
- [16] C. A. Lodi and M. Ursino, "Hemodynamic effect of cerebral vasospasm in humans: a modeling study," *Annals of biomedical engineering*, vol. 27, no. 2, pp. 257–273, 1999.
- [17] J. Alastruey, S. Moore, K. Parker, T. David, J. Peiró, and S. Sherwin, "Reduced modelling of blood flow in the cerebral circulation: coupling 1-d, 0-d and cerebral auto-regulation models," *International journal for numerical methods in fluids*, vol. 56, no. 8, p. 1061, 2008.
- [18] F. Liang, K. Fukasaku, H. Liu, and S. Takagi, "A computational model study of the influence of the anatomy of the circle of willis on cerebral hyperperfusion following carotid artery surgery," *Biomedical engineering online*, vol. 10, no. 1, p. 1, 2011.
- [19] V. Papantchev, V. Stoinova, A. Aleksandrov, D. Todorova-Papantcheva, S. Hristov, D. Petkov, G. Nachev, and W. Ovtcharoff, "The role of Willis circle variations during unilateral selective cerebral perfusion: a study of 500 circles," *European Journal of Cardio-Thoracic Surgery*, vol. 44, no. 4, pp. 743–753, 2013.
- [20] J. R. Romero, A. Pikula, T. N. Nguyen, Y. L. Nien, A. Norbash, and V. L. Babikian, "Cerebral collateral circulation in carotid artery disease," *Current cardiology reviews*, vol. 5, no. 4, pp. 279–288, 2009.
- [21] A. Angermaier, S. Langner, M. Kirsch, C. Kessler, N. Hosten, and A. V. Khaw, "CT-angiographic collateralization predicts final infarct volume after intra-arterial thrombolysis for acute anterior circulation ischemic stroke," *Cerebrovascular Diseases*, vol. 31, no. 2, pp. 177–184, 2010.
- [22] O. Y. Bang, J. L. Saver, S. J. Kim, G.-M. Kim, C.-S. Chung, B. Ovbiagele, K. H. Lee, and D. S. Liebeskind, "Collateral flow predicts response to endovascular therapy for acute ischemic stroke," *Stroke*, vol. 42, no. 3, pp. 693–699, 2011.
- [23] O. Y. Bang, J. L. Saver, S. J. Kim, G.-M. Kim, C.-S. Chung, B. Ovbiagele, K. H. Lee, D. S. Liebeskind, and Others, "Collateral flow averts hemorrhagic transformation after endovascular therapy for acute ischemic stroke," *Stroke*, vol. 42, no. 8, pp. 2235–2239, 2011.
- [24] S. J. Payne, "A model of the interaction between autoregulation and neural activation in the brain," *Mathematical biosciences*, vol. 204, no. 2, pp. 260–81, 2006.
- [25] N. Stergiopoulos, D. Young, and T. Rogge, "Computer simulation of arterial flow with applications to arterial and aortic stenoses," *Journal of biomechanics*, vol. 25, no. 12, pp. 1477–1488, 1992.
- [26] R. Fahrig, H. Nikolov, A. J. Fox, and D. W. Holdsworth, "A three-dimensional cerebrovascular flow phantom," *Medical physics*, vol. 26, no. 8, pp. 1589–1599, 1999.
- [27] P. Rothwell, M. Eliasziw, S. Gutnikov, A. Fox, D. Taylor, M. Mayberg, C. Warlow, H. Barnett, C. E. T. Collaboration *et al.*, "Analysis of pooled data from the randomised controlled trials of endarterectomy for symptomatic carotid stenosis," *The Lancet*, vol. 361, no. 9352, pp. 107–116, 2003.
- [28] G. J. Adams, D. M. Simoni, C. B. Bordon, G. W. Vick, K. T. Kimball, W. Insull, and J. D. Morrisett, "Bilateral symmetry of human carotid artery atherosclerosis," *Stroke*, vol. 33, no. 11, pp. 2575–2580, 2002.
- [29] B. Hillen, B. A. Drinkenburg, H. W. Hoogstraten, and L. Post, "Analysis of flow and vascular resistance in a model of the circle of willis," *Journal of biomechanics*, vol. 21, no. 10, pp. 807–814, 1988.
- [30] S. Moore, K. Moorhead, J. Chase, T. David, and J. Fink, "One-dimensional and three-dimensional models of cerebrovascular flow," *Journal of biomechanical engineering*, vol. 127, no. 3, pp. 440–449, 2005.
- [31] R. D. Henderson, M. Eliasziw, A. J. Fox, P. M. Rothwell, H. J. M. Barnett, and Others, "Angiographically defined collateral circulation and risk of stroke in patients with severe carotid artery stenosis," *Stroke*, vol. 31, no. 1, pp. 128–132, 2000.